Published in final edited form as:

MAGMA. 2010 April ; 23(2): 85–91. doi:10.1007/s10334-010-0202-2.

Prediction of myocardial signal during CINE balanced SSFP imaging

Kyunghyun Sung,

Department of Radiology, Lucas Center for MRI/S, Stanford University, 1201 Welch Road, Stanford, CA 94305-5488, USA

Hsu-Lei Lee,

Ming Hsieh Department of Electrical Engineering, University of Southern California, Los Angeles, CA, USA

Houchun H. Hu, and

Ming Hsieh Department of Electrical Engineering, University of Southern California, Los Angeles, CA, USA

Krishna S. Nayak

Ming Hsieh Department of Electrical Engineering, University of Southern California, Los Angeles, CA, USA

Abstract

Object—To develop a signal model for accurate prediction of myocardial signal during cine-balanced steady-state free precession (bSSFP) imaging.

Methods—We present a signal model that takes into account the effects of non-ideal slice profile, off-resonance, and radio-frequency transmit variation on myocardial signal behavior. Each of the three factors was examined over the range of imaging parameters routinely used in cine bSSFP cardiac imaging at 3Tesla.

Results—In five healthy volunteers and over a wide range of prescribed flip angles, the conventional on-resonance signal model exhibited 28.9 ± 3.9% error, while the proposed model exhibited only 2.9 ± 1.4% error, and therefore more accurate predictions of myocardial signal behavior. Slice profile effects were found to be significant and accounted for most of the improvement. Off-resonance and RF transmit inhomogeneity effects were less significant but did produce more accurate signal prediction.

Conclusions—The proposed signal model produced more accurate predictions of myocardial signal compared to existing models and can be used for the optimization of pulse sequences and protocols.

Keywords

Balanced SSFP signal model; Slice profile; RF inhomogeneity; Off-resonance

Correspondence to: Kyunghyun Sung.

A preliminary account of this work was presented at SCMR 2008 (#150).

Introduction

Improvements in signal-to-noise ratio (SNR) and contrast-to-noise ratio (CNR) often directly translate to greater diagnostic power, improved image-based analysis, and more accurate signal intensity-based quantification. In order to maximize the SNR or CNR of pulse sequences and protocols, it is important to develop signal models that accurately predict relative tissue signal intensity as a function of imaging parameters such as the prescribed flip angle and the repetition time (TR). These parameters can then be optimized within normal safety limits to produce the most SNR or CNR efficient protocols and the most diagnostically useful images.

Balanced steady-state free precession (bSSFP) (equivalently known as TrueFISP, FIESTA, or Balanced-FFE) has emerged as a powerful sequence for cardiovascular MRI because of its high SNR efficiency and strong blood/tissue contrast. It is routinely used for the assessment of left ventricular (LV) function and wall motion at 1.5 and 3T [1–3] and has also been used in a variety of other applications such as myocardial perfusion imaging [4–6] and coronary artery imaging [7]. The sequence consists of a repeating series of excitations and acquisitions where all gradients are refocused over each TR [8–10]. The theoretical characteristics of bSSFP steady-state signals have been well studied [11–13].

The SNR optimization of cine bSSFP is an important means for improving diagnostic image quality and enabling the use of parallel imaging with higher reduction factors. The optimization is typically done by choosing a flip angle based on the expected signal [14]. Accurate signal modeling is likely to be even more significant for quantitative cardiac studies such as myocardial blood oxygenation level-dependent (BOLD) SSFP or myocardial edema imaging. Measured bSSFP signals, unfortunately, do not always agree with published models [15–17], which makes sequence optimization difficult. We hypothesize that practical factors related to flip angle and spectral variation can make the ideal steady-state models less accurate and contribute to the apparent deviations between measured and predicted signals.

To the best of our knowledge, little has been reported on the differences between the myocardial signal behav-ior in theory and in measurements. In this work, we first examine several practical factors that can influence to the myocardial bSSFP signal such as a non-ideal slice profile [17], static magnetic field (B_0) inhomogeneity [18], and RF transmit field $\left(B_1^+\right)$ inhomogeneity [19,20]. Introducing the three above-mentioned factors into the signal prediction process, we then formulate an amended model that more accurately predicts myocardial signal behavior during 2D bSSFP imaging by quantitatively comparing it with the measured myocardial signal.

Materials and methods

Simplified bSSFP signal model

The steady-state bSSFP signal can be analytically derived [13,21,22]. For on-resonant tissue, the steady-state transverse magnetization (M_{ss}) at the echo time (TE)=TR/2 is:

$$M_{ss}(\alpha_n) = \frac{(1-E_1)\cdot\sqrt{E_2}}{1-(E_1-E_2)\cdot\cos\alpha_n - E_1E_2}\cdot\sin\alpha_n \quad (1)$$

where $E_{1,2} = e^{-TR/T_{1,2}}$ and α_n is the prescribed flip angle [23]. For short TR (TR $\ll T_{1,2}$), $E_{1,2}$ can be approximated as (1 − TR/$T_{1,2}$), and the steady-state formula simplifies to:

$$M_{ss}(\alpha_n) = \frac{\sin\alpha_n}{(T_1/T_2+1)-\cos\alpha_n\cdot(T_1/T_2-1)}. \quad (2)$$

This equation suggests that tissue signal is solely controlled by flip angle and that tissue signal can be maximized when the flip angle is [14]:

$$\alpha_{n,\text{optimium}} = \frac{T_1-T_2}{T_1+T_2}. \quad (3)$$

In our experience, and particularly for myocardial signal, we have found that the measured signal substantially deviates from Eq. 2, resulting in inaccurate estimation of the optimal flip angle. This suggests that Eq. 2, although theoretically correct, may be inadequate for in vivo bSSFP signal modeling. The hypothesis of our work is that the deviation in signal may be due to a non-ideal slice profile, off-resonance (B_0 inhomogeneity), and flip angle variation (B_1^+ inhomogeneity). We separately analyze the effects of each of these three factors, as described in the following sections.

Modified bSSFP signal models

Slice profile—A short TR is desirable to avoid banding artifacts in bSSFP imaging. This limits the choice of excitation RF pulses. 2D bSSFP cardiac imaging typically uses low time-bandwidth (TB) product (1.5 or 2) windowed sinc or Gaussian pulse shapes. Such pulses have a relatively smooth transition in slice profiles. The smooth transition is reflected by a corresponding distribution of actual flip angles $\alpha_n(z)$ along the slice selection direction.

Figure 1 compares the flip angle distributions with high and low TB windowed sinc RF pulses. The TB 16 pulse produces a sharp profile and relatively constant α_n, while the TB=2 pulse produces a smooth flip angle distribution rather than constant α_n. The contribution of $\alpha_n(z)$ in M_{ss} signal across the imaging slice was incorporated into the steady-state signal model as follows:

$$M_{ss,P}(\alpha_n) = \int M_{ss}(\alpha_n(z))dz. \quad (4)$$

B_0 inhomogeneity—There exists a substantial resonance frequency variation across the myocardium, largely due to susceptibility effects near the lung interference and around draining coronary veins [24–26]. In bSSFP, $M_{ss}(\alpha_n)$ behaves differently at various resonant frequencies, and the frequency response of bSSFP, $M_{ss}(\alpha_n, \Delta f)$, can be easily estimated using matrix notation [13,22]. Field mapping was performed to measure resonance offsets, Δf, and a histogram of Δf over a small region of interest (ROI) is then normalized by the total number of voxels to compute a relative signal weighting $W(\Delta f)$.

The contribution of $W(\Delta f)$ across the myocardial ROI was incorporated into the steady-state signal model as follows:

$$M_{ss,B_0}(\alpha_n) = \int M_{ss}(\alpha_n, \Delta f) \cdot W(\Delta f) \mathrm{d}\Delta f . \quad (5)$$

Note that the equation assumes the constant Δf per voxel and does not include intravoxel dephasing.

B_1^+ inhomogeneity— B_1^+ (RF transmit) inhomogeneity leads to discrepancies between the prescribed and actual flip angle, which has been well documented in cardiac imaging [19,20]. We estimated the actual flip angle $\alpha_{n,\,\mathrm{actual}}$ in the ROI for each prescribed flip angle α_n by,

$$\alpha_{n,\,\mathrm{actual}} = \alpha_n \cdot b_1 \quad (6)$$

where b_1 is a relative B_1^+ scale, measured using the saturated double angle method [20,27]. In practice, b_1 is approximately constant over small regions of myocardium (e.g. one segment in the 17-segment model). The contribution of B_1^+ inhomogeneity in the myocardial ROI was incorporated into the steady-state signal model as follows:

$$M_{ss,B_1}(\alpha_n) = M_{ss}(\alpha_{n,\,\mathrm{actual}}) . \quad (7)$$

Experimental methods

Experiments were performed on a 3Tesla Signa EXCITE HD system (GE Healthcare, Waukesha, WI) with gradients capable of 40 mT/m amplitude and 150 T/m/s slew rate. A body coil was used for RF transmission, and an 8-channel phased array cardiac coil was used for signal reception. Parallel imaging was not used. In all studies, the transmit gain, center frequency, and receive gain were calibrated using a standard pre-scan only once per volunteer, and the same values were applied throughout the exam. The center frequency was adjusted over a 3D region of interest containing the LV. Synchronization with the cardiac cycle was achieved with prospective triggering based on an electrocardiogram (ECG) signal. The Institutional Review Board of the University of Southern California approved the

imaging protocols. Each subject was screened for magnetic resonance imaging risk factors and provided informed consent in accordance with institutional policy.

Localization of long-axis and mid-short-axis slices was performed using a product real-time sequence. B_0 and B_1^+ maps [20,27] were then obtained in two separate breath-holds. Both sequences used fat saturation pre-pulses and short spiral readouts. B_1^+ maps were slightly adjusted to correct the slice profile [28]. Imaging parameters for B_0 mapping were as follows: FOV 30cm, in-plane resolution=2.6mm, TE=1.6 and 3.6=ms (±250Hz frequency range), TR=12.8ms, prescribed flip angle=30°, and slice thickness=5mm. Imaging parameters for B_1^+ mapping were as follows: FOV=30cm, in-plane resolution 5mm, TE=2ms, TR=7.2ms, prescribed flip angle=60 and 120°, and slice thickness=5mm.

Cardiac bSSFP =cine loops were acquired using a product 2D FIESTA sequence with prescribed flip angles from 10 to 90° in steps of 5°. We fixed the TR and RF pulse duration, and adjusted the RF pulse amplitude to change the prescribed flip angles. Imaging parameters were as follows: FOV=30cm, matrix=224 224, slice thickness=5mm, cardiac phases=10, views per segment=20, TR=5.0 ms (four subjects) and 5.9ms (one subject), and total=heart-beats=12. RF pulse parameters: pulse duration=1.28ms and TB=2.

Data analysis

Images from mid-diastole were selected for analysis, and the ROI used signal measurements contained septal myocardium only. For numerical simulation, the T_1 and T_2 relaxation times of a phantom were measured (T_1/T_2 = 200 ms/30 ms), and two sets of myocardial relaxation times were assumed, set A (T_1/T_2 = 1,115 ms/41 ms [14,18]) and set B (T_1/T_2 1,471 ms/47 ms [29]). All seven combinations that either considered or excluded each factor (slice profile, B_0 and B_1^+) and the simplified signal model (ignoring all three) were evaluated using a relative error metric defined as:

$$\text{Relative Error} = \frac{1}{17}\sum_{n=1}^{17}\left|\frac{\text{SI}_{\text{measured}}(\alpha_n) - \text{SI}_{\text{expected}}(\alpha_n)}{\text{SI}_{\text{measured}}(\alpha_n)}\right| \quad (8)$$

where the total number of samples was 17 (10–90° in steps of 5°). The expected signal intensity ($\text{SI}_{\text{expected}}$) was adjusted to have the same minimum and maximum range of the mean measured signal intensity ($\text{SI}_{\text{measured}}$), and then both $\text{SI}_{\text{measured}}$ and $\text{SI}_{\text{expected}}$ were normalized by the maximum $\text{SI}_{\text{measured}}$. Image analysis and Bloch simulation were performed in MATLAB 7.0 (The Mathworks, Inc., Natick, MA).

Results

The steady-state signal as a function of the prescribed flip angle (10–90°) was first tested in a Gd-doped sphere phantom (17cm diameter) in conjunction with B_0 and B_1^+ mapping. The T_1 and T_2 relaxation times of the phantom were first measured with an inversion recovery spin-echo sequence and a spin-echo sequence, respectively. In this phantom, only the effects

of a non-ideal slice profile ($M_{ss,\ P}$) were considered because the resonant offset within the ROI was close to 0Hz and the relative B_1^+ scale was close to 100% (b_1 = 97%). Figure 2a shows selected magnitude images with the different prescribed flip angles and a circular ROI. The signal intensity curves (Fig. 2b) illustrate the reduced discrepancy between the measured (mean±standard deviation (SD)) and expected signals by including the non-ideal slice profile factor (Eq. 4). Relative errors were 10.9 and 4.0% using M_{ss} and $M_{ss,\ P}$, respectively.

Figure 3 shows the inhomogeneities of B_0 and B_1^+ fields over the myocardium from one representative volunteer. Histograms of the relative resonant frequency offset $W(\Delta f)$, and the relative B_1^+ scale (b_1) within the ROI are shown in Fig. 3c and d. $W(\Delta f)$ was normalized by the total number of pixels. In this subject, the resonant offset ranged from 0 to 25Hz ($\Delta f_{max} - f_{min}$ = 21 Hz), and b_1 was 72.9%, which were used in the modified signal models, Eqs. 5 and 7, respectively. For all subjects, a frequency variation ($\Delta f_{max} - f_{min}$) was 16 ± 4Hz, and b_1 was 72.2 ± 10.4%.

Figure 4 illustrates one representative in vivo result. Magnitude images (shown in Fig. 4a) are overlapped with the manually selected ROI. The simplified on-resonance signal model shows substantial deviation from the measured values, while the modified signal model including all three practical factors (slice profiles, off-resonance, and B_1^+ inhomogeneity) was in good agreement with measured values (Fig. 4b) using the two different sets of relaxation times. In this subject, the relative errors were 33.3 and 34.7% using M_{ss}, and 1.7 and 2.5% using $M_{ss,\ P+B_0+B_1}$ with set A and B, respectively.

Figure 5 contains the mean and SD of the relative error for each signal model with two sets of relaxation times, averaged over all five subjects. All the possible combinations and the simplified steady-state signal model were evaluated because each factor independently contributes the signal deviation. The minimum relative error was 3.0 ± 1.8% (set A) and 2.9 ± 1.3% (set B) when considering all three practical factors $\left(M_{ss,\ P+B_0+B_1}\right)$, while $M_{ss,\ P}$ and $M_{ss,\ P+B_1}$ also showed excellent performance, 7.0±3.6%(set A) and 9.7±3.9%(set B), and 4.2 ± 2.2% (set A) and 3.5 ± 1.5% (set B), respectively, compared to 28.2 ± 4.3% (set A) and 29.6 ± 4.3% (set B) using M_{ss}. The relative errors using the combinations of B_0 and the other one ($M_{ss,\ P+B_0}$ and $M_{ss,\ B_0+B_1}$) were higher than the relative errors using only one factor ($M_{ss,\ P}$ and $M_{ss,\ B_1}$). This observation would suggest that consideration of B_0 with P or B_1 actually worsened the signal prediction model, but including B_0 alone actually improved performance. This is mainly because the improvements somewhat counteracted each other, which provided higher errors in some combinations.

Discussion

The study quantitatively compared the simplified steady-state formula (Eq. 2) with the measured myocardial signal as a function of the prescribed flip angle. The relative error considering both the sets of relaxation times was measured to be 28.9±3.9%, which indicates a substantial deviation from the actual measurements. The modified signal model including all three practical factors $\left(M_{\mathrm{ss},\ P+B_0+B_1}\right)$ reduced this relative error to 2.9 ± 1.4%. Among all other combinations, $M_{\mathrm{ss},\ P}$ and $M_{\mathrm{ss},\ P+B_1}$ also showed comparable results, 8.4 3.6 and 3.9 ± 1.7%, respectively, compared to $M_{\mathrm{ss},\ P+B_0+B_1}$. Although each factor was treated as a separate model, the signal models containing slice profile and B_0 inhomogeneity together ($M_{\mathrm{ss},\ P+B_0}$ and $M_{\mathrm{ss},\ P+B_0+B_1}$) include the fact off-resonance may impact the slice profile [30]. It is important to note that the non-ideal slice profile is independent of the subject, whereas both the B_0 and B_1^+ mapping requires an additional subject-based calibration. This suggests that simple incorporation of slice profile effects may dramatically improve signal prediction without the need for additional pre-scan calibration.

Recent studies have suggested that magnetization transfer (MT) can influence bSSFP signals when short TRs and large flip angles are used [16,31]. This could cause a reduction in the overall observed myocardial signal [32], which can deviate from the theoretically predicted signal. We examined the maximum range of myocardial signal changes when using six different levels of RF power with fixed TR of 5.6 ms and flip angle of 45° in the separate experiment [33]. The maximum myocardial signal changes for four healthy subjects were 12.7 ± 4.7%, while the five repeated measurements with the same imaging parameters showed 8.2 3.3% signal changes. These data suggest that the MT effects have no significant impact on the myocardial signal prediction model over the range of imaging parameters in 3T bSSFP cardiac imaging.

The behavior of the magnetization vector in bSSFP sequences strongly depends on T_1 and T_2 relaxation times. We measured T_1 and T_2 for phantom, but two different sets of T_1 and T_2 values from literature were used for myocardium at 3T [14,18,29]. Although the proposed model showed an excellent agreement with experimentally measured data, additional T_1 and T_2 measurements may further improve the accuracy of the model.

We evaluated the modified steady-state models on a 3T system, which is known to have greater B_0 and B_1^+ field inhomogeneities over the myocardium compared to 1.5T. The slice profile for a given RF pulse is expected to be independent of static field strengths, while the B_0 and B_1^+ field inhomogeneities depend on the field strength. The relative contribution of the signal model improvements will vary at different field strengths.

The issue of slice profile effects is most significant in 2D imaging. 3D bSSFP imaging typically accommodates sharp slab profiles and regions for analysis are more likely to have a uniform flip angle. Therefore, the non-idealities of the slab profile may be less prominent

and create only minor signal deviation as a function of the distance to the slab center. The effects of B_0 and B_1^+ inhomogeneity are expected to be similar for 2D and 3D bSSFP.

Only the steady-state signal intensity for myocardium has been evaluated in this study. LV blood pool signal tends to increase with prescribed flip angle, presumably because it does not reach a true steady-state in 2D imaging. To predict blood pool signal, models may require substantial modification and the inclusion of transient signal models [11,13,22, 34,35]. Other cardiac phases than mid-diastole may contain transient effects on signal due to varying slice positions, and the extension to transient signal models will also be useful to understand these signal behaviors. The full assessment of both transient and steady-state signal behavior during bSSFP imaging will be appreciated in many applications where the tissue of interest exhibits both the transient and steady-state behavior.

The excitation angle plays a critical role in achieving the maximum SNR and/or CNR in many applications. The myocardial signal in LV function imaging can be directly guided by the estimation of the optimum flip angle. The other possible applications of bSSFP pulse sequences include the first-pass myocardial perfusion imaging, arterial spin labeled (ASL) myocardial perfusion imaging, BOLD imaging, and T_2-weighted edema imaging.

Conclusion

We have demonstrated a modified model for the bSSFP signal that takes into account the effects of non-ideal slice profiles, B_0 inhomogeneity, and B_1^+ inhomogeneity, and accurately predicts myocardial signal behavior during cine bSSFP imaging. The proposed model including all the three factors shows an excellent match with experimental observations (2.9% error, compared to 28.9% error of the previous model). Each practical factor contributes the accuracy of prediction independently and, among all three factors, the non-ideal slice profile was found to be the most important one to consider, followed by B_1^+ and B_0 inhomogeneities. This suggests the inclusion of the slice profile consideration can dramatically improve the signal prediction, which can be further improved by extra B_1^+ and/or B_0 calibration scans. This improved prediction can be used to optimize myocardial SNR efficiency in cardiac bSSFP imaging.

Acknowledgments

The grant sponsor for this study was National Institutes of Health (Grant #R21-HL079987).

References

1. Thiele H, Nagel E, Paetsch I, Schnackenburg B, Bornstedt A, Kouwenhoven M, Wahl A, Schuler G, Fleck E. 2001; Functional cardiac MR imaging with steady-state free precession (SSFP) significantly improves endocardial border delineation without contrast agents. J Magn Reson Imaging. 14:362. [PubMed: 11599059]
2. Plein S, Bloomer TN, Ridgway JP, Jones TR, Bainbridge GJ, Sivananthan MU. 2001; Steady-state free precession magnetic resonance imaging of the heart: comparison with segmented k-space gradient-echo imaging. J Magn Reson Imaging. 14:230. [PubMed: 11536399]

3. Alfakih K, Thiele H, Plein S, Bainbridge GJ, Ridgway JP, Sivananthan MU. 2002; Comparison of right ventricular volume measurement between segmented k-space gradient-echo and steady-state free precession magnetic resonance imaging. J Magn Reson Imaging. 16:253. [PubMed: 12205580]
4. Atkinson DJ, Burstein D, Edelman RR. 1990; First-pass cardiac perfusion: evaluation with ultrafast MR imaging. Radiology. 174:757. [PubMed: 2305058]
5. McNamara MT, Higgins CB, Ehman RL, Revel D, Sievers R, Brasch RC. 1984; Acute myocardial ischemia: magnetic resonance contrast enhancement with gadolinium-DTPA. Radiology. 153:157. [PubMed: 6473777]
6. Schwitter J, Wacker CM, van Rossum AC, Lombardi M, AlSaadi N, Ahlstrom H, Dill T, Larsson HBW, Flamm SD, Mar-quardt M, Johansson L. 2008; MR-IMPACT: comparison of perfusion-cardiac magnetic resonance with single-photon emission computed tomography for the detection of coronary artery disease in a multicentre, multivendor, randomized trial. Eur Heart J. 29:480. [PubMed: 18208849]
7. Bi X, Deshpande V, Simonetti O, Laub G, Li D. 2005; Three-dimensional breathhold SSFP coronary MRA: a comparison between 1.5T and 3.0T. J Magn Reson Imaging. 22:206. [PubMed: 16028242]
8. Haacke EM, Wielopolski PA, Tkach JA, Modic MT. 1990; Steady-state free precession imaging in the presence of motion: application for improved visualization of the cerebrospinal fluid. Radiology. 175:545. [PubMed: 2326480]
9. Carr HY. 1958; Steady-state free precession in nuclear magnetic resonance. Phys Rev. 112:1693.
10. Oppelt A, Graumann R, Barfuss H, Fischer H, Hartl W, Schajor W. 1986; FISP? A new fast MRI sequence. Electromedica. 54:15.
11. Huang TY, Huang IJ, Chen CY, Scheffler K, Chung HW, Cheng HC. 2002; Are TrueFISP images T2/T1-weighted? Magn Reson Med. 48:684. [PubMed: 12353286]
12. Scheffler K, Lehnhardt S. 2003; Principles and applications of balanced SSFP techniques. Eur Radiol. 13:2409. [PubMed: 12928954]
13. Schmitt P, Griswold MA, Gulani V, Haase A, Flentje M, Jakob PM. 2006; A simple geometrical description of the TrueFISP ideal transient and steady-state signal. Magn Reson Med. 55:177. [PubMed: 16323155]
14. Schär M, Kozerke S, Fischer SE, Boesiger P. 2004; Cardiac SSFP imaging at 3 Tesla. Magn Reson Med. 51:799. [PubMed: 15065254]
15. Schmitt P, Griswold MA, Jakob PM, Kotas M, Gulani V, Flentje M, Haase A. 2004; Inversion recovery TrueFISP: quantification of T_1, T_2, and spin density. Magn Reson Med. 51:661. [PubMed: 15065237]
16. Bieri O, Scheffler K. 2006; On the origin of apparent low tissue signals in balanced SSFP. Magn Reson Med. 56:1067. [PubMed: 17036284]
17. Coolen B, Heijman E, Nicolay K, Strijkers G. 2009; On the use of steady-state signal equations for 2D TrueFISP imaging. Magn Reson Imaging. 26:815.
18. Noeske R, Seifert F, Rhein KH, Rinneberg H. 2000; Human cardiac imaging at 3T using phased array coils. Magn Reson Med. 44:978. [PubMed: 11108638]
19. Greenman RL, Shirosky JE, Mulkern RV, Rofsky NM. 2003; Double inversion black-blood fast spin-echo imaging of the human heart: a comparison between 1.5T and 3.0T. J Magn Reson Imaging. 17:648. [PubMed: 12766893]
20. Sung K, Nayak KS. 2008; Measurement and characterization of RF nonuniformity over the heart at 3T using body coil transmission. J Magn Reson Imaging. 27:643. [PubMed: 18306272]
21. Freeman R, Hill HDW. 1971; Phase and intensity anomalies in Fourier transform NMR. J Magn Reson. 4:366.
22. Hargreaves BA, Vasanawala SS, Pauly JM, Nishimura DG. 2001; Characterization and reduction of the transient response in steady-state MR imaging. Magn Reson Med. 46:149. [PubMed: 11443721]
23. Zur Y, Stokar S, Bendel P. 1988; An analysis of fast imaging sequences with steady-state transverse magnetization refocusing. Magn Reson Med. 6:175. [PubMed: 3367775]
24. Jaffer FA, Wen H, Balaban RS, Wolff SD. 1996; A method to improve the B0 homogeneity of the heart in vivo. Magn Reson Med. 36:375. [PubMed: 8875407]

25. Reeder SB, Faranesh AZ, Boxerman JL, McVeigh ER. 1998; In vivo measurement of T2* and field inhomogeneity maps in the human heart at 1.5T. Magn Reson Med. 39:988. [PubMed: 9621923]
26. Atalay MK, Poncelet BP, Kantor HL, Brady TJ, Weisskoff RM. 2001; Cardiac susceptibility artifacts arising from the heart-lung interface. Magn Reson Med. 45:341. [PubMed: 11180442]
27. Cunningham CH, Pauly JM, Nayak KS. 2006; Saturated double-angle method for rapid B1+ mapping. Magn Reson Med. 55:1326. [PubMed: 16683260]
28. Schär, M; Vonken, EJPA; Stuber, M. Simultaneous B0- and B1-map acquisition for fast localized shim, frequency and rf power determination in the heart at 3T. Proceedings of ISMRM, 16th annual meeting; Toronto. 2008. 358
29. Stanisz G, Odrobina E, Pun J, Escaravage M, Graham S, Bronskill M, Henkelman R. 2005; T1, T2 relaxation and magne-tization transfer in tissue at 3T. Magn Reson Med. 54:507. [PubMed: 16086319]
30. Staehle F, Leupold J, Hennig J, Markl M. 2008; Off-resonance-dependent slice profile effects in balanced steady-state free precession imaging. Magn Reson Med. 59:1197. [PubMed: 18429020]
31. Bieri O, Scheffler K. 2007; Optimized balanced steady-state free precession magnetization transfer imaging. Magn Reson Med. 58:511. [PubMed: 17763346]
32. Weber, O; Scheffler, K; Bieri, O. Magnetization transfer in cardiac TrueFISP imaging. Proceedings of ISMRM, 15th annual meeting; Berlin. 2007. 2518
33. Sung, K; Lee, HL; Hu, HH; Nayak, KS. Magnetization transfer effects in cardiac balanced SSFP imaging at 3T. Proceedings of ISMRM, 16th annual meeting; Toronto. 2008. 1401
34. Ganter C. 2004; Off-resonance effects in the transient response of SSFP sequences. Magn Reson Med. 52:368. [PubMed: 15282820]
35. Scheffler K. 2003; On the transient phase of balanced SSFP sequences. Magn Reson Med. 49:781. [PubMed: 12652552]

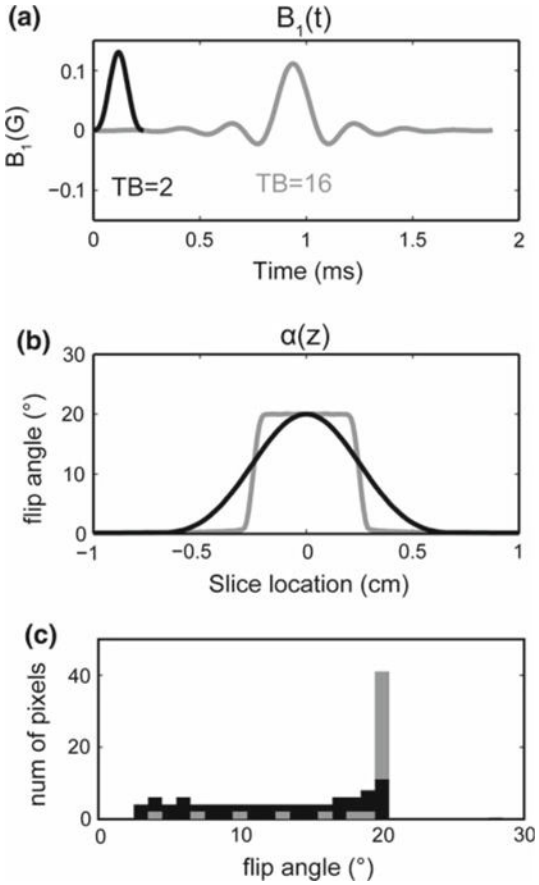

Fig. 1.

Illustration of the difference between excitation pulses with high and low time-bandwidth (*TB*) product with a desired flip angle of 20°: **a** RF pulse shapes, **b** flip angle profiles, and **c** corresponding flip angle histograms

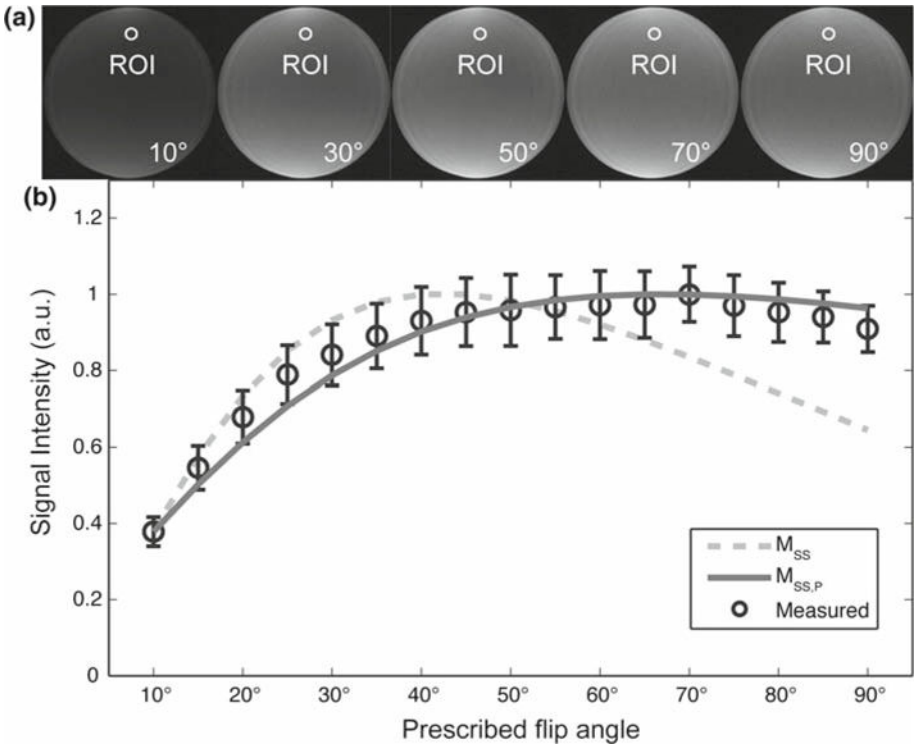

Fig. 2.

Comparison of steady-state signal models in a uniform ball phantom: **a** magnitude images and **b** signal as a function of the prescribed flip angle: (°) measured signal (mean±SD) over the ROI, (*dotted line*) predictions based on a simplified signal model, and (*solid gray line*) predictions based on a signal model that includes a non-ideal slice profile

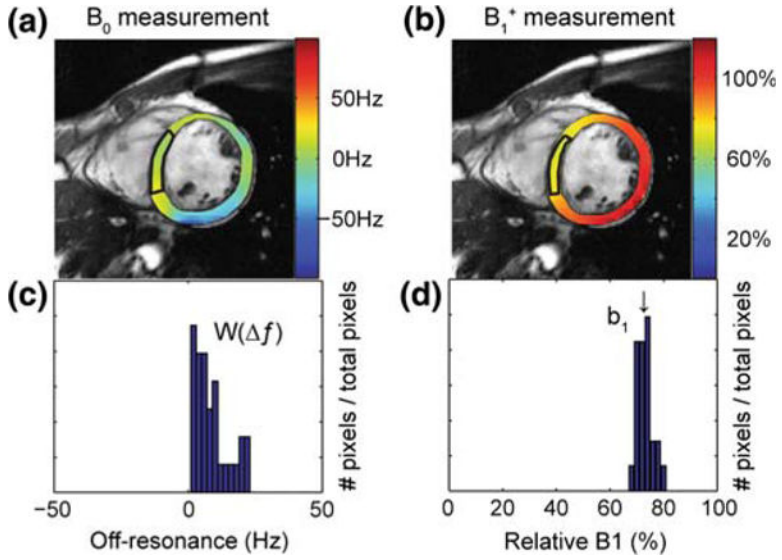

Fig. 3.

Illustration of B_0 and B_1^+ inhomogeneity in short-axis slices in one representative volunteer: **a** and **c** B_0 field map and histogram of myocardial resonance offset and **b** and **d** B_1^+ field map and histogram of relative myocardial RF amplitude (actual divided by desired). Note that the average relative B_1^+ scale (b_1) is 72.9% (*arrow*) in this subject

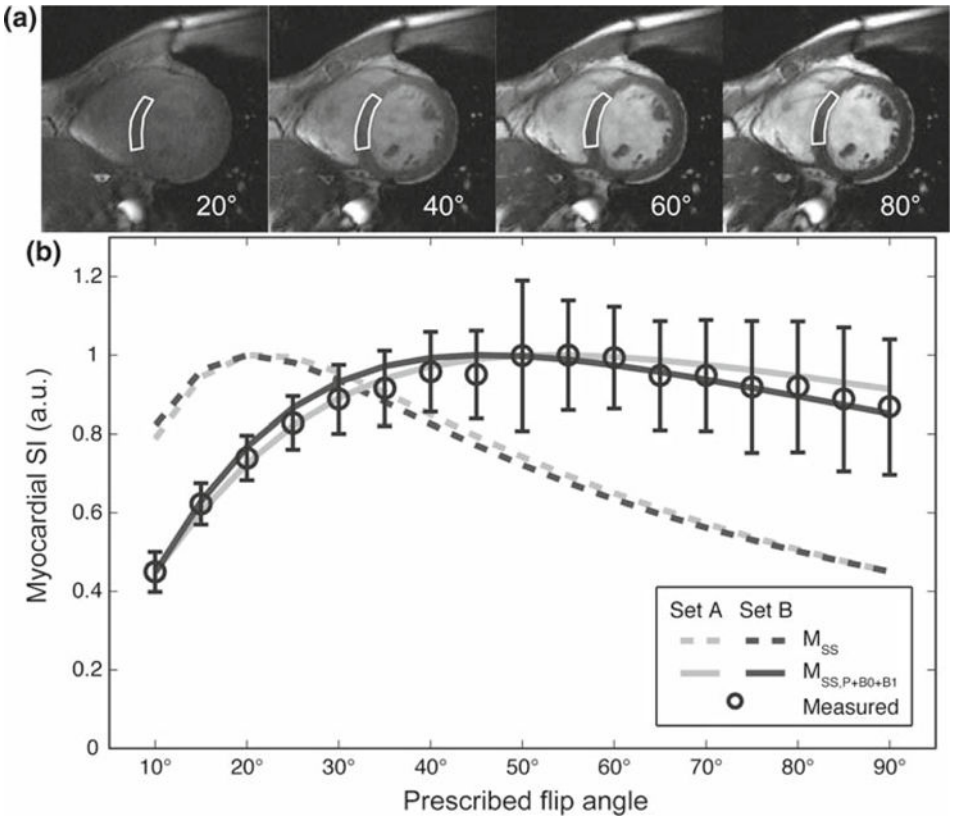

Fig. 4.

Comparison of steady-state myocardial signal models in 3T bSSFP cardiac imaging: **a** mid-diastolic images from cine acquisitions with different prescribed flip angles and **b** myocardial signal as a function of the prescribed flip angle: (°) measured signal (mean±SD) over the ROI, (*dashed lines*) predictions based on a simplified signal model, and (*solid lines*) predictions based on a signal model that includes a non-ideal slice profile, off-resonance, and RF transmit inhomogeneity

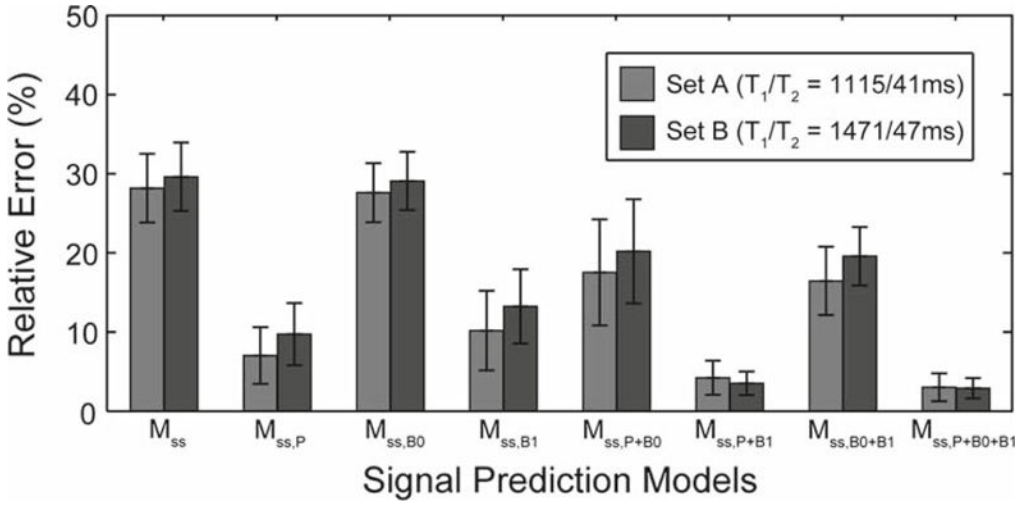

Fig. 5.

Comparison of steady-state myocardial signal prediction for all combinations of the three proposed modifications. The relative errors (mean±SD) using the two sets of relaxation times are shown for all five subjects. The simplified steady-state model exhibited 28.2 ± 4.3% (*set A*) and 29.6 ± 4.3% (*set B*) error, and the signal model including all three factors exhibited only 3.0 ± 1.8% (*set A*) and 2.9 ± 1.3% (*set B*) error